Internal Delensing of Cosmic Microwave Background Polarization B-Modes with the POLARBEAR Experiment

S. Adachi *et al.* (POLARBEAR Collaboration)

Internal delensing of cosmic microwave background polarization B-modes with the POLARBEAR experiment

S. Adachi,[1] M. A. O. Aguilar Faúndez,[2,3] Y. Akiba,[4] A. Ali,[5] K. Arnold,[6] C. Baccigalupi,[7,8,9]
D. Barron,[10] D. Beck,[11] F. Bianchini,[12] J. Borrill,[13,14] J. Carron,[15,*] K. Cheung,[5] Y. Chinone,[5,16,17]
K. Crowley,[5] H. El Bouhargani,[11] T. Elleflot,[6] J. Errard,[11] G. Fabbian,[15,†] C. Feng,[18] T. Fujino,[19]
N. Goeckner-Wald,[5] M. Hasegawa,[20] M. Hazumi,[20,16,21,4] C. A. Hill,[5] L. Howe,[6] N. Katayama,[16] B. Keating,[6]
S. Kikuchi,[19] A. Kusaka,[22,23,17,24] A. T. Lee,[5,22,25] D. Leon,[6] E. Linder,[14] L. N. Lowry,[6] F. Matsuda,[16]
T. Matsumura,[16] Y. Minami,[20] T. Namikawa,[26] M. Navaroli,[6] H. Nishino,[24] J. Peloton,[27] A. T. P. Pham,[12]
D. Poletti,[7,8,9] G. Puglisi,[28,29] C. L. Reichardt,[12] Y. Segawa,[4] B. D. Sherwin,[30] M. Silva-Feaver,[6]
P. Siritanasak,[6] R. Stompor,[11] O. Tajima,[1] S. Takatori,[4,20] D. Tanabe,[4,20] G. P. Teply,[6] and C. Vergès[11]

(The POLARBEAR collaboration)

[1]*Department of Physics, Kyoto University, Kyoto 606-8502, Japan*
[2]*Department of Physics and Astronomy, Johns Hopkins University, Baltimore, MD 21218, USA*
[3]*Departamento de Física, FCFM, Universidad de Chile, Blanco Encalada 2008, Santiago, Chile*
[4]*SOKENDAI (The Graduate University for Advanced Studies),*
Shonan Village, Hayama, Kanagawa 240-0193, Japan
[5]*Department of Physics, University of California, Berkeley, CA 94720, USA*
[6]*Department of Physics, University of California, San Diego, CA 92093-0424, USA*
[7]*International School for Advanced Studies (SISSA), Via Bonomea 265, 34136, Trieste, Italy*
[8]*Institute for Fundamental Physics of the Universe (IFPU), Via Beirut 2, 34014 Trieste, Italy*
[9]*National Institute for Nuclear Physics (INFN), via Valerio 2, 34127 Trieste, Italy*
[10]*Department of Physics and Astronomy, University of New Mexico, Albuquerque, New Mexico, USA 87131*
[11]*AstroParticule et Cosmologie (APC), Univ Paris Diderot,*
CNRS/IN2P3, CEA/Irfu, Obs de Paris, Sorbonne Paris Cité, France
[12]*School of Physics, University of Melbourne, Parkville, VIC 3010, Australia*
[13]*Computational Cosmology Center, Lawrence Berkeley National Laboratory, Berkeley, CA 94720, USA*
[14]*Space Sciences Laboratory, University of California, Berkeley, CA 94720, USA*
[15]*Department of Physics & Astronomy, University of Sussex, Brighton BN1 9QH, UK*
[16]*Kavli Institute for the Physics and Mathematics of the Universe (Kavli IPMU,*
WPI), UTIAS, The University of Tokyo, Kashiwa, Chiba 277-8583, Japan
[17]*Kavli Institute for the Physics and Mathematics of the Universe (WPI),*
Berkeley Satellite, the University of California, Berkeley, CA 94720, USA
[18]*Department of Physics, University of Illinois at Urbana-Champaign, 1110 W Green St, Urbana, IL, 61801, USA*
[19]*Yokohama National University, Yokohama, Kanagawa 240-8501, Japan*
[20]*High Energy Accelerator Research Organization (KEK), Tsukuba, Ibaraki 305-0801, Japan*
[21]*Institute of Space and Astronautical Science (ISAS),*
Japan Aerospace Exploration Agency (JAXA), Sagamihara, Kanagawa 252-0222, Japan
[22]*Physics Division, Lawrence Berkeley National Laboratory, Berkeley, CA 94720, USA*
[23]*Department of Physics, The University of Tokyo, Tokyo 113-0033, Japan*
[24]*Research Center for the Early Universe, School of Science,*
The University of Tokyo, Tokyo 113-0033, Japan
[25]*Radio Astronomy Laboratory, University of California, Berkeley, CA 94720, USA*
[26]*DAMTP, University of Cambridge, Cambridge CB3 0WA, UK*
[27]*Laboratoire de l'Accélérateur Linéaire, Université Paris-Sud, CNRS/IN2P3, Orsay, France*
[28]*Department of Physics, Stanford University, Stanford, CA, 94305*
[29]*Kavli Institute for Particle Astrophysics and Cosmology,*
SLAC National Accelerator Laboratory, 2575 Sand Hill Rd, Menlo Park, CA 94025
[30]*Kavli Institute for Cosmology Cambridge, Cambridge CB3 OHA, UK*
(Dated: February 25, 2020)

Using only cosmic microwave background polarization data from the POLARBEAR experiment, we measure B-mode polarization delensing on sub-degree scales at more than 5σ significance. We achieve a 14% B-mode power variance reduction, the highest to date for internal delensing, and improve this result to 22% by applying for the first time an iterative *maximum a posteriori* delensing method. Our analysis demonstrates the capability of internal delensing as a means of improving constraints on inflationary models, paving the way for the optimal analysis of next-generation primordial B-mode experiments.

Introduction. Inflation is a paradigm which can explain the physics of the primordial Universe. It features an early epoch of accelerated expansion during

which the primordial density perturbations as well as a generic stochastic background of gravitational waves are produced. The latter subsequently imprints a unique signature in the anisotropies of the cosmic microwave background (CMB) polarization, curl-like patterns (B-modes), most prominent on degree angular scales [1–3]. The amplitude of such a signal (usually parametrized by the tensor-to-scalar ratio r) can be related to the energy scale at which inflation took place and thus is one of the most promising probes of the physics of the early Universe [4]. However, large-scale structures (LSS) in the Universe distort the predominant gradient-like E-modes of CMB polarization (that are mainly generated by the primordial scalar perturbations) through weak gravitational lensing, creating additional B-mode polarization [5, 6] that contaminates the tensor signal.

The lensing B-modes act as a source of variance, and will soon limit primordial B-mode searches. Removing the lensing effects in CMB maps (delensing) will become a necessary data analysis step [7]. Delensing requires the subtraction of a template of the lensing B-mode signal constructed from observed E-modes and a tracer of the mass distribution that lensed the CMB. This tracer can be obtained from CMB through its lensing potential (internal delensing) or using external astrophysical data. Delensing has been demonstrated on data only recently [8–11]. A maximal reduction in B-power of 28% has been achieved using the Cosmic Infrared Background (CIB) as the lensing tracer [10, 12]. The only internal delensing attempts so far used *Planck* data and achieved a 5–7% reduction in power limited by the high noise in the tracer measurement [9, 11]. While CIB and LSS delensing will remain more powerful in the next few years, internal delensing is expected to eventually become more effective and remove the lensing B-modes almost optimally [13] when suitably low-noise data are available [14].

We report here a delensing analysis of the sub-degree B-mode signal angular power spectrum C_ℓ^{BB} of the CMB polarization experiment POLARBEAR [15, 16]. We test two types of internal lensing estimators: the standard quadratic estimator (QE) $\hat{\phi}^{QE}$ [17] and a more powerful *maximum a posteriori* (MAP) iterative method $\hat{\phi}^{MAP}$ [14, 18], applied here to data for the first time.

The reconstruction noise of CMB-internal estimates originates from random anisotropic features in the CMB maps that were interpreted as lensing. Hence, an attempt to remove the lensing features using these tracers can suppress too much anisotropy of the CMB maps. Large delensing-like signatures (called internal delensing bias), unrelated to actual delensing, can then be found in the delensed CMB spectra [9, 19, 20]. To mitigate this problem we introduce a dedicated technique applicable both to the QE and MAP estimations.

Data and simulations. We use the first two seasons of observations between 2012 and 2014, covering an effective sky area of 25 deg^2 at $3'.5$ resolution distributed over three sky patches chosen for their low foreground contamination, referred to as RA23, RA12 and RA4.5. The effective white-noise levels in the full-season coadded map of the Stokes parameters Q^{dat} and U^{dat} reach 6, 7, and $10\,\mu$K-arcmin respectively. These are among the deepest observations of CMB polarization to date at high angular resolution. This data set is well-suited for an internal delensing analysis as it provides good signal-to-noise measurements of both the lensing tracer and CMB polarization. Details of the POLARBEAR data analysis are given in Refs. [21] (PB14) and [22] (PB17). In this work we assume *Planck* 2015 [23] as our fiducial ΛCDM cosmology and use CMB maps produced with POLARBEAR pipeline A. We correct the maps for the absolute calibration, polarization efficiency and polarization angle miscalibration following PB17 before any further processing. We use Fourier modes $500 \leq \ell \leq 2500$ to construct the lensing tracers and report delensing results in four linearly spaced multipole bins between $500 \leq \ell \leq 2100$. To characterize uncertainties in our analysis we use two sets of 500 simulated POLARBEAR datasets including realistic noise and data processing effects as in PB17. The two sets share the same noise realizations but use lensed or Gaussian CMB drawn from a lensed CMB power spectrum as sky signal. We refer to these sets of simulations as non-Gaussian and Gaussian simulations respectively.

Power spectrum estimation. Following PB14 and PB17, we estimate the E and B-mode power spectra [24] from the daily Q and U maps through an inverse noise variance weighted average of their pure-pseudo cross-spectra [25, 26] accounting for the sky masking, telescope beam and data processing effects [27]. To estimate the delensed spectra we follow the same pipeline, but first subtract the templates of the lensing B-mode described below from each daily map prior to the cross-spectrum calculation. We denote the difference in power after and before delensing by $\Delta D_\ell^{BB} \equiv D_\ell^{BB,delensed} - D_\ell^{BB}$, where $D_\ell^{BB} = \ell(\ell+1)C_\ell^{BB}/2\pi$.

Quadratic estimate. From the full-season-coadded maps $X^{dat} = (Q^{dat}, U^{dat})$ we produce Wiener-filtered E and B modes $X_{\boldsymbol{\ell}}^{WF} \equiv (E_{\boldsymbol{\ell}}^{WF}, B_{\boldsymbol{\ell}}^{WF})$ in the flat-sky approximation as follows. We build pixel-space diagonal noise covariance matrices N from our noise simulations, which include inhomogeneities induced by the observing strategy. Combining this with the full effective PB17 transfer function $\mathcal{B}$ (defined as mapping the CMB E and B Fourier modes to pixelized Stokes data, including the instrument beam and processing transfer function), we have

$$X_{\boldsymbol{\ell}}^{WF} \equiv \left[\begin{pmatrix} \frac{1}{C_\ell^{EE}} & 0 \\ 0 & \frac{1}{C_\ell^{BB}} \end{pmatrix} \delta_{\boldsymbol{\ell\ell'}} + \left[\mathcal{B}^\dagger N^{-1} \mathcal{B} \right]_{\boldsymbol{\ell\ell'}} \right]^{-1} \mathcal{B}^\dagger N^{-1} X^{dat}. \tag{1}$$

This neglects the small E-to-B leakage caused by data processing as well as anisotropies in the transfer function. Both effects are included in the simulations and only result in a slight sub-optimality of the lensing tracer. We

mask pixels with estimated noise level larger than $55\,\mu$K-arcmin, and include PB17 point source masks. To reduce the internal delensing biases, we modify the N matrix by artificially assigning extra noise σ_b to every single B-mode within the multipole bin b that we try to delens. Such modes are the main contributors to the biases. We refer to this procedure as the overlapping B-modes deprojection (OBD). The N^{-1} matrix is then replaced by the $N^{-1}_{(b)}$ matrix

$$N^{-1}_{(b)} \equiv N^{-1} - N^{-1}\mathcal{T}_b \left(\frac{1}{\sigma_b^2} + \mathcal{T}_b^\dagger N^{-1}\mathcal{T}_b \right)^{-1} \mathcal{T}_b^\dagger N^{-1}, \quad (2)$$

where for every B-mode multipole $\boldsymbol{\ell}_B = \ell_B e^{i\phi_{\boldsymbol{\ell}_B}}$ within a multipole bin $[\mathcal{T}_b]_{Q(\boldsymbol{x}_i)\boldsymbol{\ell}_B} = \sin 2\phi_{\boldsymbol{\ell}_B} e^{i\boldsymbol{\ell}_B\cdot\boldsymbol{x}_i}$ and $[\mathcal{T}_b]_{U(\boldsymbol{x}_i)\boldsymbol{\ell}_B} = \cos 2\phi_{\boldsymbol{\ell}_B} e^{i\boldsymbol{\ell}_B\cdot\boldsymbol{x}_i}$. The complete masking of these modes is achieved only for infinite σ_b^2 but in this case the inversion of the bracketed matrix in Eq. (2) becomes numerically unstable. To avoid this, we chose a high, but finite, noise amplitude $\sigma_b = 1000\,\mu$K-arcmin to sufficiently down-weight them. Using $\sigma_b = 100\,\mu$K-arcmin does not change our results. Eq. (1) is then evaluated with a simple conjugate gradient solver. From these filtered maps an unnormalized quadratic estimate of the CMB lensing Fourier modes $\hat{g}_{\boldsymbol{L}}$ is built following Ref. [18], using the minimum variance combination of the EE and EB estimators (in the fiducial model). At the POLAR-BEAR level of sensitivity, the polarization data provide a CMB lensing reconstruction noise lower than that achievable using temperature data on all angular scales. The EB estimator in particular has the lowest noise in RA23 and RA12 sky patches. The estimate is then normalized and Wiener-filtered as $\hat{\phi}^{\mathrm{QE,WF}}_{\boldsymbol{L}} = \epsilon_L N^{(0)}_L (\hat{g}_{\boldsymbol{L}} - \langle\hat{g}_{\boldsymbol{L}}\rangle_{\mathrm{MC}})$, where $\epsilon_L \equiv C^{\phi\phi,\mathrm{fid}}_L/(C^{\phi\phi,\mathrm{fid}}_L + N^{(0)}_L)$, $N^{(0)}_L$ is the QE reconstruction noise level [28] as predicted from the central noise levels of the patches, their effective transfer functions, CMB E and B multipole cuts. $C^{\phi\phi,\mathrm{fid}}_L$ is our fiducial lensing potential power spectrum. This isotropic normalization is adequate in the patch centers where delensing is most efficient, but results in a slight down-weighting of the tracer towards the edges where the noise is higher. Finally, $\langle\hat{g}_{\boldsymbol{L}}\rangle_{\mathrm{MC}}$ is the 'mean-field' used to subtract sources of anisotropies unrelated to lensing [29] obtained by averaging 200 simulations. ϵ_L may be interpreted as a naive estimator of the scale-dependent delensing efficiency in the patch centers [12]. OBD trades delensing efficiency for lower delensing biases. In RA23 this reduces ϵ_L by $\sim35\%, 20\%, 10\%$ and 5% for our four bins, compared to no deprojection. This issue is less severe for experiments aiming at delensing degree-scale B-modes as in this case the modes to exclude are restricted to the largest scales, which carry little information for the lensing potential reconstruction.

Iterative estimate. The construction of the MAP lensing estimate follows closely Ref. [18] (with the addition of OBD), which can be briefly summarized as follows: at each iteration step, the filter in Eq. (1) is replaced with a similar filter with vanishing C^{BB}_ℓ but which includes the lensing deflection estimate in $\mathcal{B}$. This reconstructs a partially delensed CMB. Then, a quadratic estimator with modified weights corrected by a mean-field term is used to capture residual lensing from these new maps. Our treatment of the mean-field is simpler than Ref. [18]. The mean-field is small at the scales of interest, and its re-evaluation at each step and band-power bin for each simulation realization is expensive. Thus, we use the same mean-field computed for $\hat{\phi}^{QE}$ at all steps. We perform 3 iterations after which we see no significant improvement.

Lensing B-mode templates. For each $\hat{\phi}_{\boldsymbol{L}}$ estimate, we build a B-mode template synthesizing first the $\hat{\phi}$ map, the polarization map $P^{(E^t)} = Q^{(E^t)} + iU^{(E^t)}$ from an E-mode template (E^t) and then projecting the remapped polarization template $P^{(E^t)}(\hat{n} + \nabla\hat{\phi}(\hat{n}))$ into B-modes (B^t). For E^t we use the $E^{\mathrm{WF}}_{\boldsymbol{\ell}}$ solution of Eq. (1) without any B-mode deprojection and apply the multipoles cuts $500 \leq \ell_E \leq 2500$. The excluded multipoles contribute 10% of the lensing B-mode power in our lowest bin $\ell_B \sim 500$ [30], and percent-level at higher ℓ_B. The impact on our delensing efficiency is thus minor. All lensing multipoles $L \leq 100$ are cut from the lensing map. This removes all scales where the mean-field is large compared to the signal, but does not affect the delensing capability of the tracer.
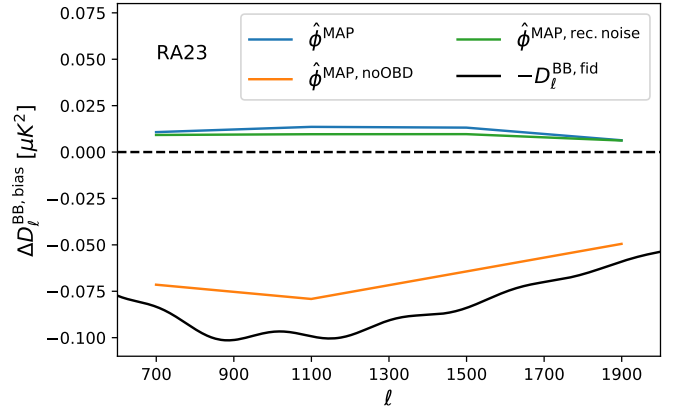

FIG. 1. Total delensing bias (defined as the result of the internal delensing operation applied to Gaussian CMB simulations) in our $\hat{\phi}^{\mathrm{MAP}}$ analysis (blue) of RA23. The contribution due to the noise of $\hat{\phi}^{\mathrm{MAP}}$ acting on the E-mode template is shown in green. The delensing bias one would obtain without the overlapping B-modes deprojection (orange) approaches the amplitude of D^{BB}_ℓ of our fiducial cosmology (black), mimicking perfect delensing.

Internal delensing bias. B^t is built out of three CMB fields: E^t, E^{WF}, and B^{WF}, where the last two are used to estimate $\hat{\phi}_{\boldsymbol{L}}$. In a standard QE implementation the leading contribution to the internal delensing bias (though

not all of it at low noise levels [31]) is sourced by the disconnected (Gaussian) correlation functions involving four CMB fields. The leading contributing terms in the spectrum ($(B^{\mathrm{dat}} - B^t)^2$, schematically) have the form $\left(E^t \star \hat{\phi}^{\mathrm{noise}}(E^{\mathrm{WF}}, B^{\mathrm{WF}})\right) \cdot B^{\mathrm{dat}}$, where $\star$ denotes the template building operation, $\cdot$ the cross-spectrum between the template and the data and $\hat{\phi}^{\mathrm{noise}}$ being the noise of the lensing tracer reconstructed using the EB estimator. Following Ref. [9] we compute the delensing bias as $\Delta \hat{D}_{\ell_b}^{\mathrm{BB,bias}} \equiv \langle \Delta \hat{D}_{\ell_b}^{\mathrm{BB}} \rangle_G$, where $\langle \cdot \rangle_G$ denotes that the entire internal delensing operation is performed on Gaussian simulations, and averaged over. Since the simulations are Gaussian, the estimated lensing tracers are pure noise, and this term captures these disconnected correlators. In Fig. 1 we show the MAP $\Delta \hat{D}_{\ell_b}^{\mathrm{BB,bias}}$ for the RA23 data (the QE curves are similar). If no OBD is performed we see a strong negative signal similar to our negative fiducial D_ℓ^{BB}, creating the illusion of an almost perfect delensing (orange). OBD prevents correlating overlapping modes in B^{WF} and B^{dat}, reducing the entire bias by almost an order of magnitude (blue). Were the tracer noise statistically independent of the map being delensed, we would only see the (positive) B-power induced by the remapping of $P^{(E^t)}$ by the tracer noise (green). This contribution can be quantified by delensing each simulation realization with an independent MAP tracer. The dominant residual contribution to the delensing bias after OBD is mostly sourced by this term, owing to B-modes at $\ell_B > 2500$ leaking to lower ℓ_B in both B^{WF} and B^{dat} due to the presence of the mask which convolves different angular scales. We verified this directly with the help of another, simpler set of simulations where all modes above $\ell_B > 2500$ were artificially zeroed-out prior the analysis.

Results. We build debiased band-powers according to

$$\Delta \hat{D}_{\ell_b}^{\mathrm{BB,debiased}} = \Delta \hat{D}_{\ell_b}^{\mathrm{BB}} - \Delta \hat{D}_{\ell_b}^{\mathrm{BB,bias}}. \qquad (3)$$

In Fig. 2 we show the inverse-variance weighted combination of $\Delta \hat{D}_\ell^{\mathrm{BB,debiased}}$ in the POLARBEAR patches. Table I shows the values of the amplitude $\Delta A^{\mathrm{delens}}$ of the simulation predictions of $\Delta \hat{D}_{\ell_b}^{\mathrm{BB,debiased}}$ fit to the data. By construction, these band-powers are in practice free of the internal delensing bias, and $\Delta A^{\mathrm{delens}} = 0$ in the absence of lensing signatures in the data. For the patch-combined measurement, we detect a non-zero $\Delta A^{\mathrm{delens}}$ with a significance $\Delta A^{\mathrm{delens}}/\sigma_{\Delta A^{\mathrm{delens}}}$ of 5σ using $\hat{\phi}^{\mathrm{QE}}$, consistent with simulation predictions ($\Delta A^{\mathrm{delens}} = 1$). The significance of the patch-combined measurement increases to 5.3σ using $\hat{\phi}^{\mathrm{MAP}}$. Our deepest patch RA23 alone provides a 4σ measurement. In all cases, $\Delta A^{\mathrm{delens}}$ agrees with expectations from simulations (shown as dashed line in Fig. 2), where the MAP delensing always outperforms QE. While MAP delensing does increase the significance of our results, we see evidence for the improvement over QE in the data only at modest signifi-
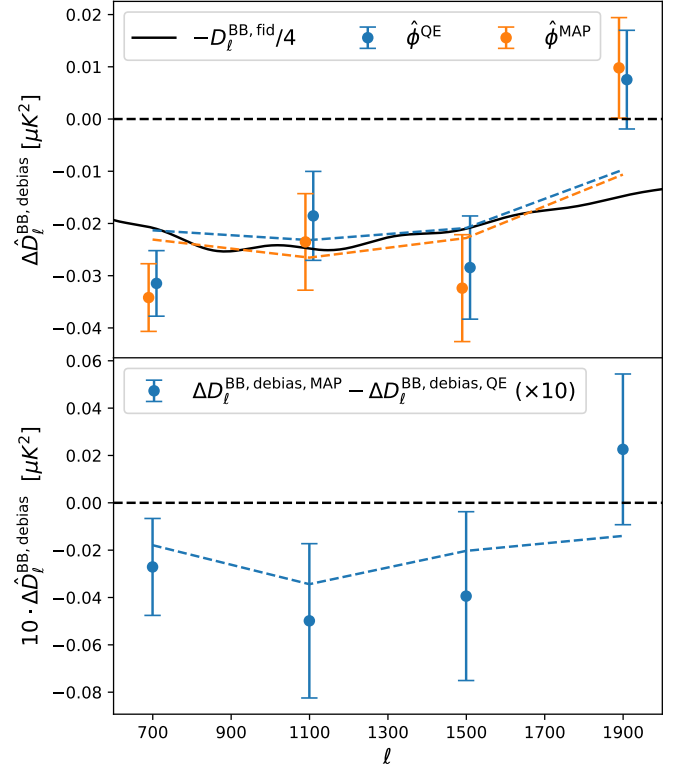

FIG. 2. *Top*: inverse-variance combination of the debiased spectral differences $\Delta \hat{D}_\ell^{\mathrm{BB,debiased}}$ measured in the POLAR-BEAR sky patches using QE (blue) and MAP (orange) delensing. The dashed lines show expectations obtained as average of results computed on simulations. *Bottom*: difference between MAP and QE delensed $\Delta \hat{D}_\ell^{\mathrm{BB,debiased}}$ compared to simulation expectations (dashed). As both these quantities are highly correlated, the error bar of this statistic is significantly reduced when compared to those of the top panel. The significance of this difference being non-zero is 2.1σ.

$\Delta \hat{D}_{\ell_b}^{\mathrm{BB,debiased}}$	$\Delta A^{\mathrm{delens}}[\hat{\phi}^{\mathrm{QE}}]$	$\Delta A^{\mathrm{delens}}[\hat{\phi}^{\mathrm{MAP}}]$
RA23	1.26 ± 0.33	1.38 ± 0.32
RA12	1.16 ± 0.39	1.09 ± 0.37
RA4.5	0.79 ± 0.59	0.59 ± 0.57
Patch-combined	1.22 ± 0.24	1.24 ± 0.23

TABLE I. Fit of the amplitude $\Delta A^{\mathrm{delens}}$ of the simulation prediction to the debiased delensed spectrum difference $\Delta \hat{D}_{\ell_b}^{\mathrm{BB,debiased}}$. Error bars were calculated using the Gaussian simulation set. A non-zero delensing signal is measured at more than 5σ after combining the data of all patches, consistent with simulation predictions ($\Delta A^{\mathrm{delens}} = 1$).

cance. The difference of $\Delta \hat{D}_{\ell_b}^{\mathrm{BB,debiased}}$ computed with MAP and QE is non-zero at 2.1σ significance, consistent with simulation expectations. The fluctuations in this statistic are caused by the decoherence of the MAP-delensed and QE-delensed maps sourced by the slightly different noise components in the tracers. A deviation

from zero of this difference is thus sourced by a difference in the delensed signal.

How much lensing B-mode power variance did we actually remove? The debiasing procedure subtracts B-power that acts as a source of additional variance in parameter inference. Hence, the relevant quantity is the reduction of power without any debiasing[1]. We find a reduction of B-power of 14% ($\hat{\phi}^{\mathrm{QE}}$) and 22% ($\hat{\phi}^{\mathrm{MAP}}$) for our deepest patch RA23, in agreement with simulation expectations ($(13 \pm 9)\%$ and $(15 \pm 9)\%$ respectively for its mean value). It is more difficult to distinguish the QE from the MAP result without debiasing on real data or on a single realization of the simulations. The observed difference between MAP and QE is thus measured at only 1.1σ, down from 2.1σ when performing debiasing. For MAP, RA12 and RA4.5 achieved a 15% and 1% power reduction consistent with QE results.

Robustness and consistency tests. We test the consistency between $\Delta\hat{D}_{\ell_b}^{\mathrm{BB}}$ of data and simulations using templates built with different tracers. We subtract from $\Delta\hat{D}_{\ell_b}^{\mathrm{BB}}$ measured on the data the average of the same quantity computed with the non-Gaussian simulations $\left\langle \Delta\hat{D}_{\ell_b}^{\mathrm{BB}} \right\rangle$, and fit to these band-powers the amplitude parameter ΔA^{BB} of the fiducial binned $-D_\ell^{\mathrm{BB}}$. By construction, $\Delta A^{\mathrm{BB}} = 0$ indicates a delensed B-power consistent with simulation expectations. We also build χ^2's from $\Delta\hat{D}_{\ell_b}^{\mathrm{BB}}$ as follows: with $\Sigma_{bb'}$ the covariance of $\Delta\hat{D}_{\ell_b}^{\mathrm{BB}}$ computed from the non-Gaussian simulations, we compute the data χ^2 across all multipole bins b

$$\chi^2 \equiv \sum_{b,b'} \left(\Delta\hat{D}_{\ell_b}^{\mathrm{BB}} - \left\langle \Delta\hat{D}_{\ell_b}^{\mathrm{BB}} \right\rangle \right) \Sigma_{bb'}^{-1} \left(\Delta\hat{D}_{\ell_{b'}}^{\mathrm{BB}} - \left\langle \Delta\hat{D}_{\ell_{b'}}^{\mathrm{BB}} \right\rangle \right),$$
(4)

that we turn into probability-to-exceed (PTE) values from the empirical ranking of the data χ^2 compared to the results obtained for the simulations. Part of the noise and cosmic variance cancels in $\Delta\hat{D}_{\ell_b}^{\mathrm{BB}}$, and this spectral difference is constrained about four times better (empirically) than the band-powers themselves. In addition to $\hat{\phi}^{\mathrm{QE}}$, $\hat{\phi}^{\mathrm{MAP}}$, and $\hat{\phi}^{\mathrm{MAP}} - \hat{\phi}^{\mathrm{QE}}$ tracers, we used $\hat{\phi}^{\mathrm{QE}}$ removing modes $L > 500$ ($\hat{\phi}^{\mathrm{QE,lowpass}}$) to assess the impact of unmodeled tracer noise. To test for delensing bias we used a QE tracer $\hat{\phi}^{\mathrm{QE,noOBD.}}$ built without OBD. Furthermore, we used tracers uncorrelated or anti-correlated with LSS such as the lensing curl mode estimate $\hat{\omega}$ [33–35] (expected to be pure noise at our noise levels), $-\hat{\phi}^{\mathrm{QE}}$ and a QE tracer $\hat{\phi}^{\mathrm{QE,indep.}}$ estimated from an independent simulation. This is independent from the map to

delens, but has otherwise the same statistical properties. All these should produce no delensing and an increase of B-power after template subtraction.

Table II shows the summary of our tests. ΔA^{BB} amplitudes show no visible bias with respect to our simulations but we observe PTE values below 5%, notably in RA23. As all these tests are correlated we assessed the significance of these low PTEs simulating 20,000 realizations of all the band-powers included in our test suites starting from their empirical covariance matrix estimated from our non-Gaussian simulations, and repeating the χ^2 analysis. We found that the probability of observing three PTEs lower than 4% in our test suite is 11% and thus concluded that our data's low PTEs are not significant.

Galactic foregrounds and systematics. Polarized dust emission could affect delensing, for example by adding Gaussian power to the tracer noise, and hence reducing the delensing efficiency. Since the dust angular power spectrum falls sharply with multipole ℓ and we use only $\ell_B \geq 500$, we expect this effect to be small. The lensing estimator could also capture specific trispectra signatures in the highly non-Gaussian dust emission, which would propagate in lensing reconstruction and, later, delensing if uncorrected for. Preliminary studies suggest that at 150 GHz this effect is not important [36]. It is implausible for such a signature to match the LSS deflection field; so this would also act to reduce the delensing efficiency. We quantified the expected impact of small-scale Gaussian polarized dust emission in our measurement by adding to our simulated data sets a template of this emission at our frequency produced with the *Model 1* of the PySM package [37], itself based on *Planck* Commander templates [38]. Comparing simulated $\Delta\hat{D}_{\ell_b}^{\mathrm{BB}}$ with and without dust we found a bias smaller than 1% of the statistical error in all multipole bins. We ignored polarized Galactic synchrotron contamination as it is subdominant in PB17 [22]. Instrumental systematics effects in the POLARBEAR measurements of D_ℓ^{BB} and QE reconstruction were found to be negligible with respect to statistical uncertainties [22, 39].

Conclusions. Our analysis has achieved the highest internal B-mode delensing efficiencies to date, and is the first where the lensing tracer has been built from CMB polarization alone, serving as a proof of concept for future experiments where CMB polarization rather than temperature power will dominate the lensing tracer sensitivity. This work provided the first demonstration on deep polarization data that superior delensing efficiencies can indeed be achieved using iterative delensing methods [14, 18]. This is a crucial step towards an efficient exploitation of future high-sensitivity B-mode polarization experiments of the next decade [40–42], for which iterative methods will provide close-to-optimal constraints on the physics of inflation [13].

We thank Antony Lewis for discussion and

---

[1] This is not always the case for internal delensing performed at the degree-scale, where both the residual power and variance carry a strong r-dependence that has to be carefully characterized [13, 32]). Our bias is sourced by high-ℓ_B noise with no cosmological dependence.

$\Delta\hat{D}_{\ell_b}^{\mathrm{BB}} - \left\langle\Delta\hat{D}_{\ell_b}^{\mathrm{BB}}\right\rangle$	RA23 ΔA^{BB}	RA12 ΔA^{BB}	RA4.5 ΔA^{BB}	RA23 PTE	RA12 PTE	RA4.5 PTE
$\hat{\phi}^{\mathrm{QE}}$	0.01 ± 0.12 (0.13)	0.09 ± 0.13 (0.10)	-0.02 ± 0.15 (0.05)	4%	60%	58%
$\hat{\phi}^{\mathrm{MAP}}$	0.07 ± 0.12 (0.15)	0.04 ± 0.14 (0.11)	-0.05 ± 0.15 (0.06)	4%	84%	75%
$\hat{\phi}^{\mathrm{QE,lowpass}}$	-0.01 ± 0.10 (0.13)	0.08 ± 0.12 (0.10)	-0.02 ± 0.13 (0.07)	16%	39%	77%
$\hat{\phi}^{\mathrm{MAP}} - \hat{\phi}^{\mathrm{QE}}$	0.04 ± 0.04 (0.01)	-0.07 ± 0.04 (0.02)	-0.04 ± 0.04 (0.02)	47%	17%	70%
$\hat{\phi}^{\mathrm{QE,noOBD}}$	-0.01 ± 0.16 (1.10)	0.01 ± 0.19 (1.09)	-0.20 ± 0.22 (1.04)	14%	80%	76%
$\hat{\omega}^{\mathrm{QE}}$	-0.18 ± 0.12 (-0.18)	-0.11 ± 0.13 (-0.14)	0.22 ± 0.13 (-0.10)	13%	3%	22%
$-\hat{\phi}^{\mathrm{QE}}$	0.05 ± 0.19 (-0.42)	-0.29 ± 0.18 (-0.29)	0.07 ± 0.17 (-0.19)	7%	14%	46%
$\hat{\phi}^{\mathrm{QE,indep.}}$	0.06 ± 0.10 (-0.13)	0.03 ± 0.10 (-0.10)	-0.05 ± 0.11 (-0.06)	62%	5%	98%

TABLE II. Consistency tests between delensing observed on data $\Delta\hat{D}_{\ell_b}^{\mathrm{BB}}$ and simulations expectations $\langle\Delta\hat{D}_{\ell_b}^{\mathrm{BB}}\rangle$ for different lensing tracers. For each patch we show the results of the fit of the amplitude ΔA^{BB} of our fiducial $-D_\ell^{\mathrm{BB}}$ to $\Delta\hat{D}_{\ell_b}^{\mathrm{BB}} - \langle\Delta\hat{D}_{\ell_b}^{\mathrm{BB}}\rangle$, as well as the χ^2 PTEs for the consistency of such quantity with a null power spectrum. ΔA^{BB} fitted to $\langle\Delta\hat{D}_{\ell_b}^{\mathrm{BB}}\rangle$ (which includes the delensing bias) is shown in parenthesis. $\Delta A^{\mathrm{BB}} > 0$ means a reduction of B-power.

[*] Corresponding author. J.Carron@sussex.ac.uk
[†] Corresponding author. G.Fabbian@sussex.ac.uk

[1] U. Seljak and M. Zaldarriaga, Phys. Rev. Lett. **78**, 2054 (1997), arXiv:astro-ph/9609169.
[2] M. Kamionkowski, A. Kosowsky, and A. Stebbins, Phys. Rev. Lett. **78**, 2058 (1997), arXiv:astro-ph/9609132.
[3] A. G. Polnarev, Sov. Astron. **29**, 607 (1985).
[4] M. Kamionkowski and E. D. Kovetz, Annu. Rev. Astron. Astrophys. **54**, 227 (2016), arXiv:1510.06042.
[5] A. Lewis and A. Challinor, Phys. Rept. **429**, 1 (2006), arXiv:astro-ph/0601594.
[6] U. Seljak and C. M. Hirata, Phys. Rev. D **69**, 043005 (2004), arXiv:astro-ph/0310163.

[2] www.cosmosnet.it
[3] web.infn.it/CSN4/IS/Linea5/InDark
[4] https://github.com/bthorne93/PySM_public
[5] https://github.com/carronj/LensIt
[6] https://github.com/cmbant/lenspix

[7] M. Kesden, A. Cooray, and M. Kamionkowski, Phys. Rev. Lett. **89**, 011304 (2002), arXiv:astro-ph/0202434.

[8] P. Larsen, A. Challinor, B. D. Sherwin, and D. Mak, Phys. Rev. Lett. **117**, 151102 (2016), arXiv:1607.05733.

[9] J. Carron, A. Lewis, and A. Challinor, J. Cosmol. Astropart. Phys. **1705**, 035 (2017), arXiv:1701.01712.

[10] A. Manzotti *et al.*, Astrophys. J. **846**, 45 (2017), arXiv:1701.04396.

[11] N. Aghanim *et al.* (Planck collaboration), Accepted for publication in Astron. Astrophys. (2020), arXiv:1807.06210.

[12] B. D. Sherwin and M. Schmittfull, Phys. Rev. D **92**, 043005 (2015), arXiv:1502.05356.

[13] J. Carron, Phys. Rev. D **99**, 043518 (2019), arXiv:1808.10349.

[14] C. M. Hirata and U. Seljak, Phys. Rev. D **67**, 043001 (2003), arXiv:astro-ph/0209489.

[15] K. Arnold *et al.*, in *Proc. SPIE Int. Soc. Opt. Eng.*, Vol. 8452 (2012) p. 84521D, arXiv:1210.7877.

[16] Z. D. Kermish *et al.*, in *Proc. SPIE Int. Soc. Opt. Eng.*, Vol. 8452 (2012) p. 84521C, arXiv:1210.7768.

[17] W. Hu and T. Okamoto, Astrophys. J. **574**, 566 (2002), arXiv:astro-ph/0111606.

[18] J. Carron and A. Lewis, Phys. Rev. D **96**, 063510 (2017), arXiv:1704.08230.

[19] W.-H. Teng, C.-L. Kuo, and J.-H. Proty Wu, (2011), arXiv:1102.5729.

[20] N. Sehgal, M. S. Madhavacheril, B. Sherwin, and A. van Engelen, Phys. Rev. D **95**, 103512 (2017), arXiv:1612.03898.

[21] P. A. R. Ade *et al.* (POLARBEAR collaboration), Astrophys. J. **794**, 171 (2014), arXiv:1403.2369.

[22] P. A. R. Ade *et al.* (POLARBEAR collaboration), Astrophys. J. **848**, 121 (2017), arXiv:1705.02907.

[23] P. A. R. Ade *et al.* (Planck collaboration), Astron. Astrophys. **594**, A13 (2016), arXiv:1502.01589.

[24] M. Zaldarriaga and U. Seljak, Phys. Rev. D **55**, 1830 (1997), arXiv:astro-ph/9609170.

[25] K. M. Smith and M. Zaldarriaga, Phys. Rev. D **76**, 043001 (2007), arXiv:astro-ph/0610059.

[26] J. Grain, M. Tristram, and R. Stompor, Phys. Rev. D **79**, 123515 (2009), arXiv:0903.2350.

[27] E. Hivon, K. M. Górski, C. B. Netterfield, B. P. Crill, S. Prunet, and F. Hansen, Astrophys. J. **567**, 2 (2002), arXiv:astro-ph/0105302.

[28] T. Okamoto and W. Hu, Phys. Rev. D **67**, 083002 (2003), arXiv:astro-ph/0301031.

[29] D. Hanson and A. Lewis, Phys. Rev. D **80**, 063004 (2009), arXiv:0908.0963.

[30] G. Fabbian and R. Stompor, Astron. Astrophys. **556**, A109 (2013), arXiv:1303.6550.

[31] T. Namikawa, Phys. Rev. D **95**, 103514 (2017), arXiv:1703.00169.

[32] T. Namikawa and R. Nagata, J. Cosmol. Astropart. Phys. **1510**, 004 (2015), arXiv:1506.09209.

[33] G. Pratten and A. Lewis, J. Cosmol. Astropart. Phys. **1608**, 047 (2016), arXiv:1605.05662.

[34] G. Fabbian, M. Calabrese, and C. Carbone, J. Cosmol. Astropart. Phys. **2018**, 050 (2018), arXiv:1702.03317.

[35] G. Marozzi, G. Fanizza, E. Di Dio, and R. Durrer, J. Cosmol. Astropart. Phys. **2016**, 028 (2016), arXiv:1605.08761.

[36] A. Challinor *et al.*, J. Cosmol. Astropart. Phys. **2018**, 018 (2018), arXiv:1707.02259.

[37] B. Thorne, J. Dunkley, D. Alonso, and S. Næss, Mon. Not. R. Astron. Soc. **469**, 2821 (2017), arXiv:1608.02841.

[38] R. Adam *et al.* (Planck collaboration), Astron. Astrophys. **594**, A10 (2016), arXiv:1502.01588.

[39] M. A. O. Aguilar Faúndez *et al.* (POLARBEAR collaboration), submitted to Astrophys. J. (2019), arXiv:1911.10980.

[40] K. N. Abazajian *et al.* (CMB-S4), (2016), arXiv:1610.02743.

[41] P. Ade *et al.* (Simons Observatory collaboration), J. Cosmol. Astropart. Phys. **2019**, 056 (2019), arXiv:1808.07445.

[42] A. Suzuki *et al.* (LiteBIRD collaboration), J. Low Temp. Phys. **193**, 1048 (2018), arXiv:1801.06987.